Annual Glacier Mass Balance on Thana Glacier

2024-2025

Cryosphere Services Division

National Center for Hydrology and Meteorology

2025

Prepared by:

Arun Puri, Hydro-met officer, apuri@nchm.gov.bt

Tshewang Jamtsho, Hydro-met officer, tjamtsho@nchm.gov.bt

Amber Bdr. Rana, Hydro-met officer, abrana@nchm.gov.bt

Published by: National Centre for Hydrology and Meteorology, Royal Government of Bhutan

PO Box: 2017

Thimphu, Bhutan

List of acronyms:

- MSI – Multispectral Instrument
- RTK – Real-Time Kinematic
- GNSS – Global Navigation Satellite System
- mm w.e. a^{-1} – Millimeter Water Equivalent per Annum
- DEM – Digital Elevation Model
- IDW – Inverse Distance Weighting
- AGMB – Annual Glacier Mass Balance
- CGMB – Cumulative Glacier Mass Balance
- ICIMOD – International Centre for Integrated Mountain Development
- TCS7 – Trimble Controller Series 7
- WGS 84 – World Geodetic System 1984
- WMO – World Meteorological Organization
- CSV – Comma-Separated Values
- IPCC – Intergovernmental Panel on Climate Change
- Gt – Gigatonnes
- m.a.s.l. – meters above sea level

Executive Summary

This technical report documents the 2024–2025 annual glacier mass-balance assessment of Thana Glacier, one of the three benchmark glaciers in the headwaters of Chamkhar chu in Bumthang Dzongkhag. The primary objective is to quantify recent glacier change—specifically glacier-wide mass balance and terminus position—using an in-situ geodetic method consistent with the national long-term monitoring framework implemented by the Cryosphere Services Division (CSD), National Center for Hydrology and Meteorology (NCHM).

Deploying high-precision Real-Time Kinematic (RTK) GNSS techniques (Trimble R10-2) and geodetic analysis, the study focused on assessing surface elevation changes and terminus recession for the year 2025. The methodology included a detailed digital elevation model (DEM) construction, DEM differencing, and hypsometric analysis within 50 m elevation bands to quantify elevation change and mass loss with accuracy. Using a combination of satellite imagery and field measurements enabled more accurate glacier boundary mapping, which in turn improved the robustness of the mass-balance estimates.

Results indicate substantial net mass loss during the 2024–2025 glaciological year. The glacier-wide annual mass balance is estimated as −1581.676 ± 231.07 mm w.e. a^{-1}, confirming continued negative mass balance within the long-term monitoring record. Over 2016–2025, the glacier recorded a cumulative mass loss of −19,484.98 mm w.e. (≈ −19.48 m w.e.), indicating sustained net thinning across the decade.

Spatial patterns of change show widespread surface lowering, with the Δh distribution centered on negative values and a mean elevation difference of −2.54 m across the glacier. Elevation-band analysis demonstrates pronounced altitudinal control: thinning is strongest at lower elevations (e.g., −3.44 m in the 5133 m – 5183 m elevation band) and decreases toward the upper sections of the glacier (e.g., −0.834 m in the 5533 to 5583 m elevation band), consistent with enhanced ablation at the tongue and moderate losses at higher elevations. Hypsometry exerts a first-order control on the glacier-wide signal because area is concentrated in the mid-elevation zone; notably, the 5183 – 5233 m band contains ~24% of total area and contributes disproportionately to the area-averaged mass balance estimation.

The one-year terminus recession between 2024 and 2025 ranges from 10.1 to 51.74 m (mean ~23.9 m), while cumulative retreat between 2023 and 2025 increases to 17.4 – 103.53 m (mean

~49.4 m; ~24.7 m a^{-1} when annualized), demonstrating sustained multi-year withdrawal of the ice front rather than an isolated positional shift. Collectively, these findings reinforce Thana Glacier's ongoing negative mass-balance regime and continued geometric adjustment. This report not only contributes to Bhutan's long-term glacier dataset but also provides actionable scientific evidence for national climate resilience planning and international reporting.

Table of Contents

List of acronyms:

Executive Summary

List of Figures

List of Tables

1. Introduction 1

2. Aim and Objective 3

3. Study Area 3

3.1. Location 3

3.2. Accessibility 3

4. Data and Methodology 4

4.1. Data Acquisition 4

4.2. Data Post Processing 5

4.2.1. Overview of approach 5

4.2.2. Datasets and inputs 6

4.2.3. Pre-processing and quality control 7

4.2.4. Interpolation of dGPS points onto a 1 m grid (IDW) 8

4.2.5. Grid definition and neighborhood search 8

4.2.6. IDW formulation and assumptions 8

4.2.7. Co-location of survey periods and elevation change computation (Δh) 9

4.2.8. Elevation changes at matched points 9

4.2.9. DEM vertical bias check and correction 9

4.2.10. Glacier hypsometry (area–elevation distribution) 10

4.2.11. Elevation-band aggregation of Δh and robust smoothing 11

4.2.12. Snow depth–elevation model and $\Delta S(z)$ 12

4.2.13. Conversion to mass balance (point-wise and area averaged) 13

5. Uncertainty Assessment **14**
5.1. Area averaged mass balance uncertainty 14
6. Results and Discussion **15**
6.1. Area averaged mass balance and uncertainty 15
6.2. Elevation-dependent surface lowering and hypsometric control 17
6.3. Glacier area change 18
6.4. Mass-balance gradient and ELA interpretation (2024–2025) 19
6.5. Cumulative terminus recession 20
7. References **22**
8. Annexture **24**
8.1. Annex A: Hypsometric elevation-band statistics and point mass balance 24
8.2. Annex B: Physical Assumptions 25
8.3. Annex C: Unit equivalence used in mass-balance calculations 25
8.4. Annex D: Snow and ice density uncertainty in mass-balance calculations. 26

List of Figures

Figure 1. Location of Thana at the headwaters of Chamkhar chu within the Chamkhar chu sub-basin). The background is a Sentinel-2 True Color Composite draped over a hillshade (70% transparency). 4

Figure 2. A) dGPS survey tracks. B) Base set up. 5

Figure 3. Workflow for glacier mass balance measurement. 6

Figure 4. A) Observed difference in the field-based surface elevation and the satellite obtained elevation. B) Bias corrected DEM 10

Figure 5. Hypsometry for the year 2024 and 2025 12

Figure 6. Glacier surface elevation changes between 2024 and 2025 generated using dGPS elevation differencing 13

Figure 7. Cumulative mass balance and annual mass balance over the observed periods 18

Figure 8. Distribution of glacier surface elevation change between 2024 and 2025. 19

Figure 9. Equilibrium-line altitude (ELA) for 2024 and 2025.Observed point mass balance (mm w.e.) versus elevation (m a.s.l.), with solid line as linear fit and dotted line showing extrapolation 22

Figure 10. Cumulative terminus positions of Thana Glacier from 2023 to 2025. The progressive upstream displacement of the terminus outline 23

List of Tables

Table 1. Cumulative Glacier Mass Balance 17

1. Introduction

Bhutan contains approximately 700 glaciers (BGI, 2018). The glaciers are the long-term relics of the legacy of past climatic conditions and one of the most sensitive pointers of any climate fluctuations and long-term changes in climate. They develop and maintain themselves where the accumulation of snowfall surpasses the melting at multi-decadal, and they preserve the freshwater in an icy state and discharge it at a seasonal duration by melting. The glaciers and ice sheets form the largest reservoir of fresh water on Earth, containing approximately 69% of the total fresh water in the world, and their continued depletion thus has significant impacts on water resources, hazards, and global sea level rise (NSDI, 2021; WGMS, n.d.).

Accelerated mass loss has become intense in the past century, and losses have been experienced at an exceptionally rapid pace in the 20th and 21st centuries as the world temperature increases because of anthropogenic greenhouse-gas forcing (Barry, 2006; IPCC, 2023). According to the recent global measurements, the mass loss of glaciers is not only extensive but also on the rise: according to a community intercomparison estimate, glaciers all around the world lost approximately ~273 ± 16 Gt per year during 2000–2023, and the loss rate was accelerating towards the end of the record (The GlaMBIE Team, 2025). Previous satellite-based syntheses had also been found to show global glacier losses of ~267 ± 16 Gt per year during 2000–2019 (Hugonnet et al., 2021). In line with these scientific evaluations, the World Meteorological Organization has highlighted over the last few years the constant extraordinary loss in glacier mass as part of its annual climate report (WMO, 2025).

The Himalaya-High Mountain Asia region, commonly known as the "Third Pole", due to the vast amount of ice at high altitudes, is home to tens of thousands of glaciers which are important in the maintenance of river systems and water security of the mountains. Multiple studies have reported large and spatially uneven mass loss in glaciers of High Mountain Asia during the satellite era, and the mass was commonly decreased at low altitudes (Brun et al., 2017; Shean et al., 2020). Other climatic evaluation reports of warming in Asia have also documented a nearly double of the global average, which is likely to raise the possibilities of more powerful melting seasons, lower snow cover, and faster glacier melting (WMO, 2025). Projected and observed variability of the balance of glacier masses in the Himalayas in particular, there is an acute sensitivity to an increase in temperature, and it determines the sustainability of glaciers in the long term and hydrology downstream (Kraaijenbrink et al., 2017).

Glaciers are a major source of freshwater, particularly in dry months when precipitation is minimal and meltwater is a vital part of river discharge. In High Mountain Asia, river systems fed by glaciers and snows provide the downstream populations and economic domains that are of significant size (Immerzeel et al., 2010). Some of the more recent international studies of water towers also underline the fact that most of the essential mountain water-source areas are also susceptible to climatic and socio-economic stressors, and that it is imperative to have a well-developed monitoring and adaptability planning on it (Immerzeel et al., 2020). The hydropower generation, agriculture and drinking-water supplies are tightly linked to glacier meltwater in Bhutan, where intense topography and deep seasonality determine water supplies, and rivers in the dry season (November-April) rely on glaciers. The ongoing glacier retreat is thus a key strategic national issue, and it has the possible impact on the seasonal water security and climate-related risk in glaciated basins.

Due to the significance of sustained observations, the Cryosphere Services Division (CSD) of the National Center of Hydrology and Meteorology (NCHM) has made a long-term glacier monitoring program, benchmarked in-situ mass balance measurement of Gangju La, Thana, and Shodug glaciers (NCHM, 2018). The benchmarking method gives a combination of field data and geodetic data (e.g., RTK-GNSS surveys, DEM generation and differencing, hypsometric analysis) as a measure of the mass change of the glacier on an annual basis, change in glacier elevation, and dynamics of terminus. Similar measurements also offer critical baseline demonstrations to clarify changing cryospheric risks (including glacial-lake formation and downstream flooding threat) that are becoming more observed in Bhutan and the Himalaya region as a whole (Sato et al., 2022; Wangchuk et al., 2024). Under this national framework, Thana Glacier, in the northern region of the Central Bhutan Himalayas as a part of the Chamkhar Chhu system continues to be a support area of critical benchmarking glacier change and enhancing Bhutan's long-term cryosphere record. This Thana Glacier 2024-2025 technical report further builds upon that work by recording the work done on the annual assessment based on the existing NCHM protocols and better scientific circumstances through recent literature.

2. Aim and Objective

The primary aim of this study is to assess recent changes in the mass balance and terminus position through in-situ based geodetic method, thereby contributing to Bhutan's long-term glacier monitoring and climate adaptation efforts.

3. Study Area

3.1. Location

Thana glacier, a clean type glacier, is located in the Northern part of Central Bhutan Himalaya (28° 57' 11" N, 90° 21' 17" E). Its elevation ranges from 5100 m.a.s.l to 5700 m.a.s.l covering an area approximately about 3km2, sourcing Chamkhar Chhu.

3.2. Accessibility

Thana glacier can be accessed via two options; the first route is via Dhur- Tshampa- Thana, which takes seven days on foot to reach the study site. The other route is via Choekhor Toe-Tshampa- Thana and takes six days on foot to reach the study site. Autumn season is a favorable season to visit the site as the glaciers in the Eastern frontier of the Bhutan Himalayas are summer accumulation type leading to excess snow cover on the glacier surface intervening the installation of mass balance stakes on the glacier surface.

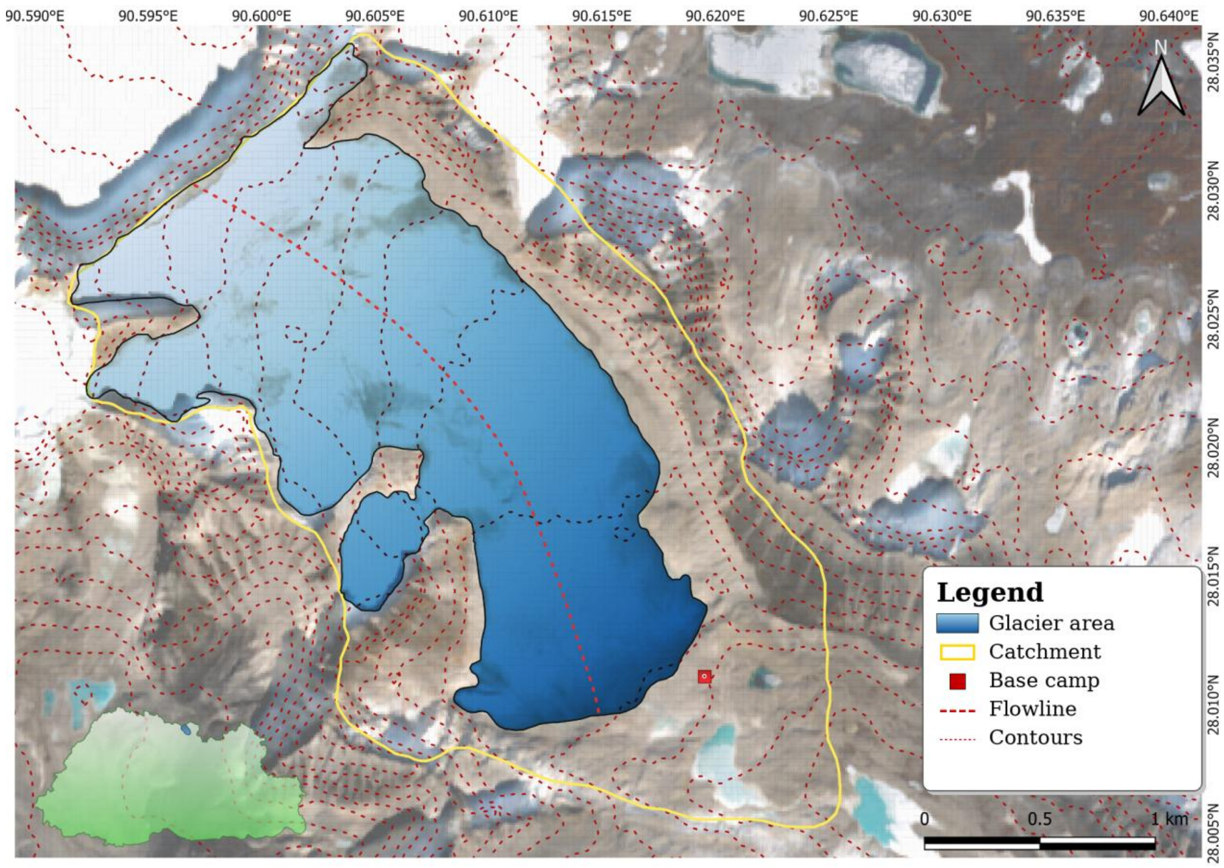

Figure 1. Location of Thana at the headwaters of Chamkhar chu within the Chamkhar chu sub-basin). The background is a Sentinel-2 True Color Composite draped over a hillshade (70% transparency)

4. Data and Methodology

4.1. Data Acquisition

Thana glacier has an in-situ based geodetic mass balance record since 2016. During the field expedition, glacier surface elevation data were collected using RTK GNSS (Trimble R10-2). Prior to the survey, Trimble R10-2 was calibrated for higher precision to avoid errors. The base station was set up accurately on the previously marked point (reference point), which is at a certain distance away from the glacier snout and kept at the height of 2 m from the ground. Manually inserting the known coordinate of base station in TCS7 controller of Trimble R10-2, base station was set to start for the collection of data. A rover was mounted on a backpack and the height of the rover from the ground was measured and entered in the controller accordingly. The logging distance of 1m with a logging interval of one second was set for all survey profiles in continuous Topo mode. Glacier surface elevations data were collected by walking across the glacier following the survey track file (shape file) of the previous year. Several new points were collected for future reference.

Similarly, glacier terminus data were collected by walking on the glacier, following the snout of the glacier for that given point of time. Unlike glacier surface elevations, there is no reference to previous year's data to walk through it. Glacier terminus either advances or recedes-in most cases they recede. Therefore, a profile along the current terminus position is taken by walking along the terminus of the glacier and compared with the previous terminus profile line to determine the changes in terminus position of the glacier.

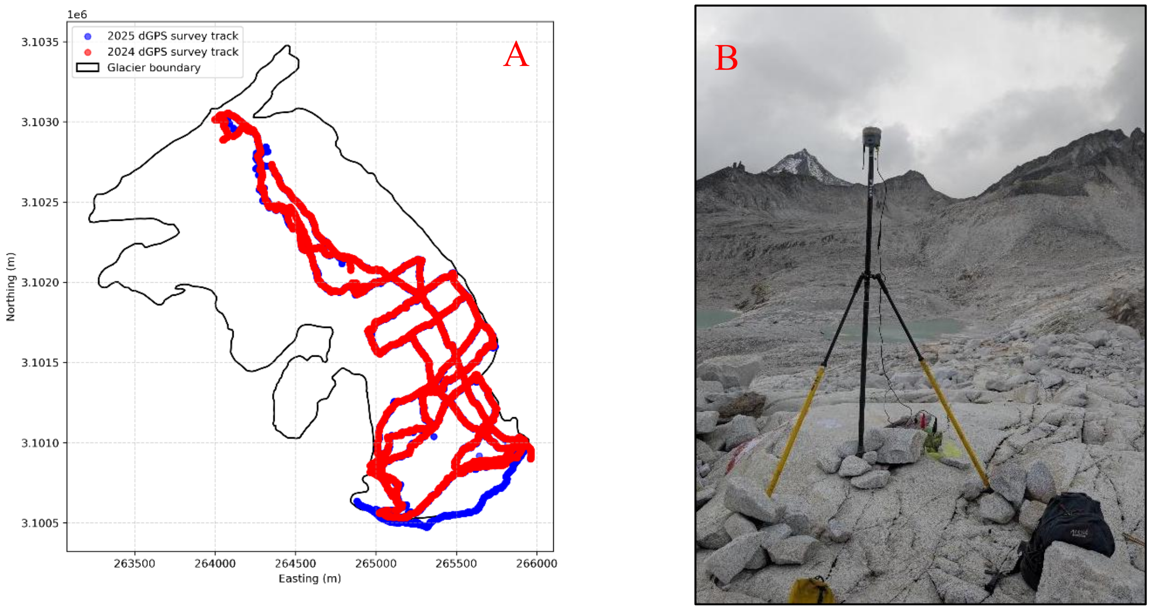

Figure 2. A) dGPS survey tracks. B) Base set up.

4.2. Data Post Processing

4.2.1. Overview of approach

The flowchart provides an overview of the workflow used to derive area averaged mass balance using an in-situ geodetic approach. It combines the surface elevation difference between the previous year (t1) and the current year (t2) from dGPS surveys with DEM bias correction, glacier hypsometry, and snow-depth modelling, followed by area-weighted integration and uncertainty assessment to estimate area averaged mass balance. All the calculations closely follow established geodetic mass-balance concepts applied in the first in-situ record of decadal glacier mass balance (2003-2014) from the Bhutan Himalaya study by Tshering and Fujita (2016).

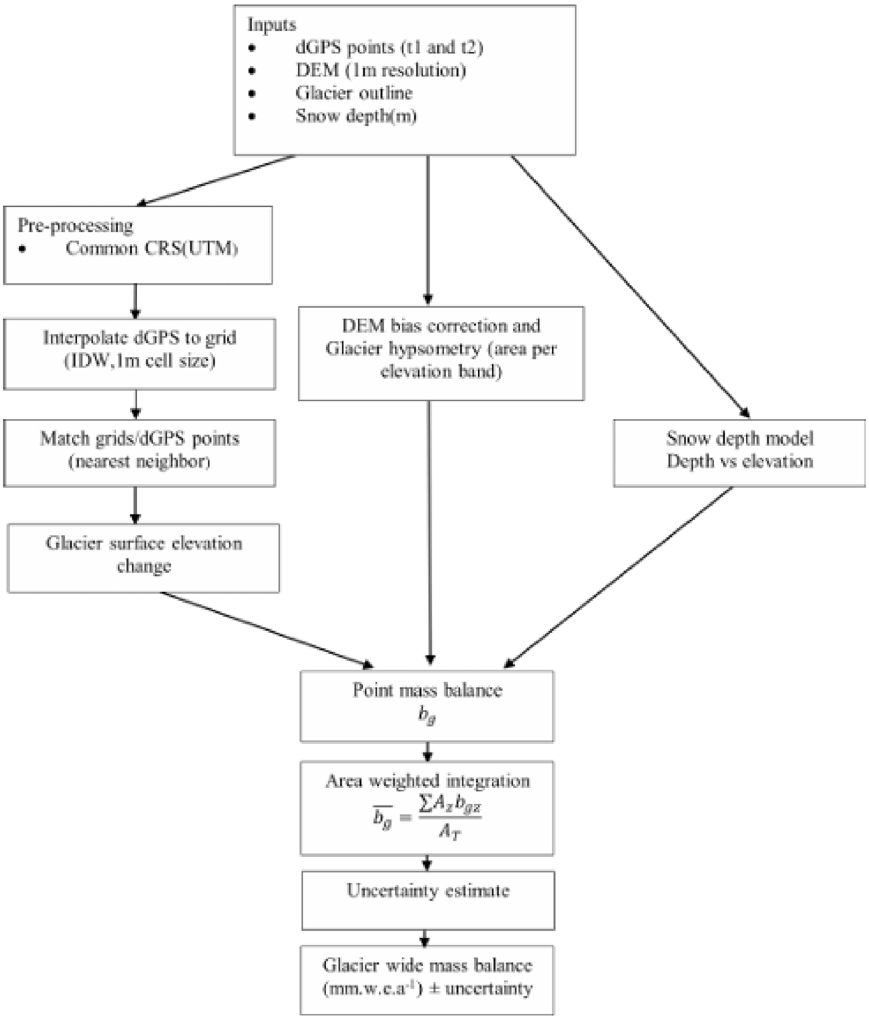

Figure 3. Workflow for glacier mass balance measurement.

4.2.2. Datasets and inputs

Glacier surface elevations measured using dGPS surveys acquired at two years, representing time period 1 (t1: previous year) and time period 2 (t2: current year) were treated as direct observations of the glacier surface elevation at the time of each survey and were used as the primary input for estimating surface elevation change between the two periods.

DEM and glacier outline

To delineate the glacier boundary, a recent Sentinel-2 median composite image (2025; 10 m resolution) was used, and the glacier outline was manually digitized in QGIS. Field-based dGPS glacier surface elevation points were then used for quality control and to apply a vertical bias correction to the 1 m DEM (Maxar) acquired a few years earlier. The corrected DEM, clipped to the mapped glacier extent using the glacier outline polygon, was subsequently used to derive glacier hypsometry (area distribution by elevation bands) and to ensure all terrain analyses were restricted to the glacier area.

Snow depth

Snow depth information and an elevation obtained at the mass balance stakes collected on two survey dates were used to estimate the snow thickness at a mid-elevation of every 50m elevation band.

Software and processing environment

Remote sensing data preparation and geospatial preprocessing were carried out using a combination of cloud-based and desktop GIS tools alongside Python. A Sentinel-2 median composite (2025; 10 m) was extracted using Google Earth Engine (GEE) to support glacier boundary identification. The glacier outline was then manually delineated in QGIS, which was also used for study area mapping. Subsequent data processing and analysis were implemented in Python using standard scientific and geospatial libraries. Numerical computation and tabular data handling were performed with NumPy and Pandas, while figures and plots were produced using Matplotlib. Vector geospatial operations (e.g., handling glacier outlines, point geometries, and spatial joins) were carried out using GeoPandas, with Shapely used for geometry construction and manipulation. Raster-based DEM processing, including reading and masking/clipping to the glacier boundary, was conducted using Rasterio (including rasterio.mask). Robust trend fitting for elevation-dependent modelling (e.g., Δh–elevation relationships) was implemented using TheilSenRegressor from scikit-learn.

4.2.3. Pre-processing and quality control

All input dGPS survey files were first imported from CSV format and checked to ensure the required coordinate and elevation fields (x, y, z) were present. The coordinate and elevation values were then converted to numeric format, and any records containing missing, non-finite, or otherwise invalid values (e.g., NaN) were removed to prevent errors in subsequent processing. Prior to any spatial analysis, all datasets and spatial layers were verified to be referenced in a common coordinate system (UTM Zone 46N) to ensure positional consistency during interpolation, clipping, and overlay operations. Finally, unit consistency was enforced across the workflow, with both horizontal coordinates and vertical elevations expressed in meters, ensuring compatibility between dGPS measurements, DEM data, and derived outputs.

4.2.4. Interpolation of dGPS points onto a 1 m grid (IDW)

To enable consistent spatial pairing between survey periods and support elevation differencing, the irregularly spaced dGPS surface elevation points were interpolated onto a regular 1 m grid using Inverse Distance Weighting (IDW). Prior to interpolation, the dGPS coordinates and elevations (x, y, z) were validated by converting values to numeric type and removing any records containing missing or non-finite entries to prevent propagation of errors into the gridded product.

4.2.5. Grid definition and neighborhood search

A regular grid was generated in UTM Zone 46N using the minimum and maximum bounds of the cleaned dGPS coordinates. For each grid node, neighboring dGPS observations were identified within a 0.7 m search radius using a cKDTree-based neighborhood query to ensure computationally efficient spatial searches. Grid nodes with no neighbors inside the search radius were retained as no-data during interpolation and excluded from the exported output.

4.2.6. IDW formulation and assumptions

Inverse Distance Weighting (IDW) is based on the spatial autocorrelation assumption that nearby locations are more similar than distant ones. For each grid node, the predicted elevation is computed as a distance-weighted average of surrounding dGPS measurements within a defined local search neighborhood. In this workflow, a search neighborhood was used and only points within a 0.7 m radius contributed to the prediction, which both reflects the expected local continuity of glacier surface elevations at meter-scale.

For a grid node at location x, the interpolated elevation $\hat{z}(x)$is given by:

$$\hat{z}(x) = \frac{\sum_{i=1}^{n} w_i z_i}{\sum_{i=1}^{n} w_i}, w_i = \frac{1}{d_i^p} \quad (1)$$

where $z_i$are observed elevations, $d_i$are distances from the grid node to each neighbor point, and p is the power parameter ($p = 2$ in our study, i.e., inverse-distance-squared weighting). Increasing p causes weights to decay more rapidly with distance, making predictions more strongly influenced by the closest points; conversely, low p values yield smoother surfaces with broader influence from neighbors. If an observation coincides exactly with a grid node ($d_i = 0$), the grid node is assigned that measured value directly, consistent with IDW behaving as an exact interpolator at sample locations.

4.2.7. Co-location of survey periods and elevation change computation (Δh)

To quantify surface elevation change between the two-survey year, the gridded (interpolated) elevation points from current year ($t2$) were spatially co-located with those from previous year ($t1$) prior to differencing. Co-location was performed using a nearest-neighbor spatial join, where each point in the $t2$ dataset was assigned the geographically closest point from the $t1$ dataset based on planimetric distance in the common projected CRS (UTM Zone 46N). An initial broad search cap (e.g., up to 50 m) can be applied to avoid unmatched points in sparse areas and to ensure that point neighbors are identified; however, the final matched dataset was restricted using a stricter acceptance criterion to maintain positional comparability. Specifically, only pairs satisfying a maximum nearest-neighbor distance of $d_{nearest} \leq 3\,m$ were retained for analysis. This distance threshold ensures that elevation change is computed only where both survey years represent nearly the same surface location and reduces the risk of introducing spurious Δh values caused by mismatched terrain, interpolation artifacts, edge effects near the glacier margin, or differences in point density between surveys.

4.2.8. Elevation changes at matched points

For each accepted matched pair, the surface elevation change was computed as:

$$\Delta h = h_{t2} - h_{t1} \tag{2}$$

where h_{t2} and h_{t1} represent co-located elevations for the current and previous year, respectively.

4.2.9. DEM vertical bias check and correction

To minimize systematic elevation offsets in the reference DEM arising from the time gap between DEM acquisition and the study period, a vertical bias correction was performed prior to hypsometric analysis by directly comparing DEM elevations with field-measured dGPS surface elevations. The DEM was first sampled at the dGPS point coordinates, and the elevation residuals were computed as:

$$\Delta z_{DEM-dGPS} = z_{DEM} - z_{dGPS} \tag{3}$$

A single representative vertical bias was then estimated from these residuals (using the mean difference as a first-order approximation) and applied uniformly across the DEM to obtain a corrected elevation surface;

$$z_{DEM,corr} = z_{DEM} - bias. \tag{4}$$

This correction step reflects the broader requirement in geodetic workflows that DEM-based analyses must account for potential vertical offsets to avoid propagating systematic errors into elevation-change and mass-balance estimates. Figure 4A and 4B show the comparison between the dGPS raw data and the Maxar-derived DEM before and after bias correction.

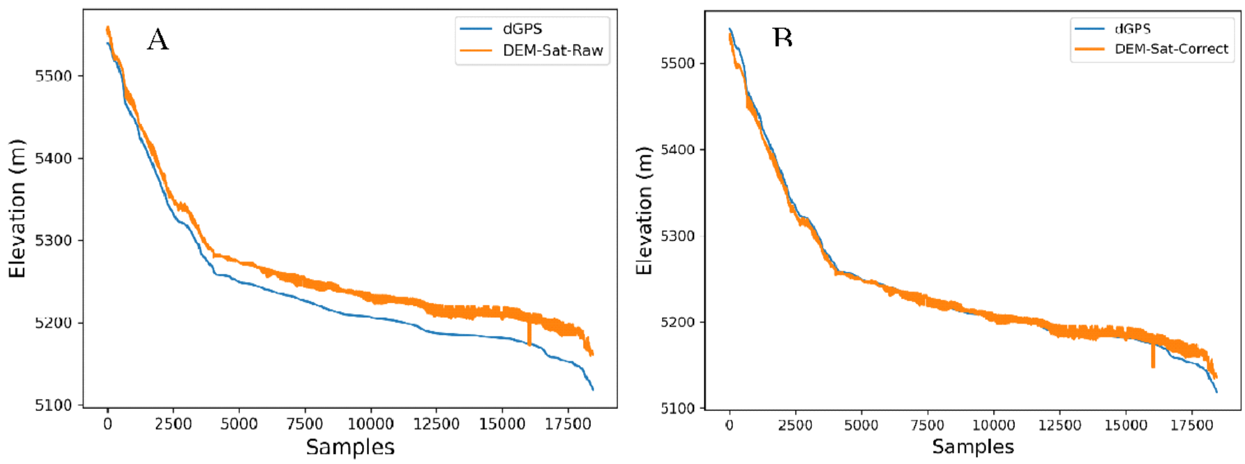

4.2.10. Glacier hypsometry (area–elevation distribution)

Glacier hypsometry (the glacier area distribution with elevation, Figure 5) was derived from the vertically corrected DEM to support elevation-band based integration of mass balance. First, the corrected DEM was clipped using the glacier outline polygon, ensuring that subsequent terrain analysis included only glacier pixels within the mapped boundary. The glacier DEM was then classified into discrete elevation bands using a 50 m interval. For each elevation band z, the glacier area A_z was computed as:

$$A_z = N_z r^2 \tag{5}$$

where r is the DEM pixel size in meters and N_z is the number of DEM pixels falling within that band z.

Where glacier extents differed between the two measurement years, the band-wise area was represented using the mean of the two, following Tshering and Fujita (2016). Specifically, for each 50 m elevation band, the representative area was computed as:

$$A_z = (A_{t1} + A_{t2})/2 \tag{6}$$

where A_{t1} and A_{t2} are the glacier areas (m²) within the same elevation band derived from the outlines corresponding to the surveys at $t1$ and $t2$, respectively. This averaged hypsometry was subsequently used for area-weighted integration of elevation-band mass balance, where $A_z$represents the area in the 50 m band (m²).

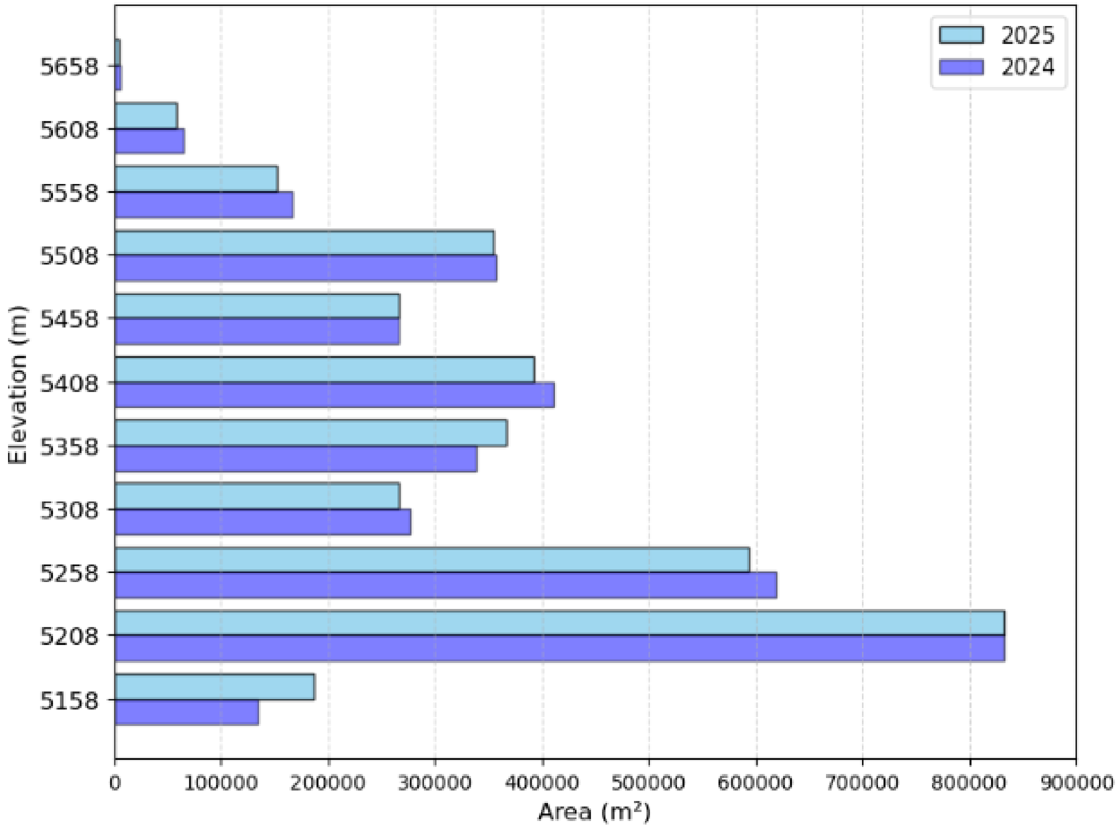

Figure 5. Hypsometry for the year 2024 and 2025

4.2.11. Elevation-band aggregation of Δh and robust smoothing

Following co-location of the two-survey period, the elevation-change observations (*Δh*) were averaged by elevation to obtain a stable, hypsometry-compatible representation of surface change across the glacier. Each matched *Δh* point was assigned to the same 50 m elevation-band scheme used for glacier hypsometry, based on its elevation. For each elevation band, the mean *Δh* was used as an initial estimate of elevation change within that band. This band-wise aggregation reduces small-scale spatial noise and ensures that elevation change is expressed in a form suitable for subsequent area-weighted integration.

Δh was modelled as a function of elevation using Theil–Sen robust regression (Figure 6), which estimates the trend based on the median of pairwise slopes and is therefore substantially less sensitive to outliers than ordinary least squares regression. The resulting fitted function, *Δh(z)* ≈ *f(z)* was then used to evaluate a missing mean *Δh* for the mid elevation band, which was used in the subsequent hypsometric integration and mass-balance calculations.

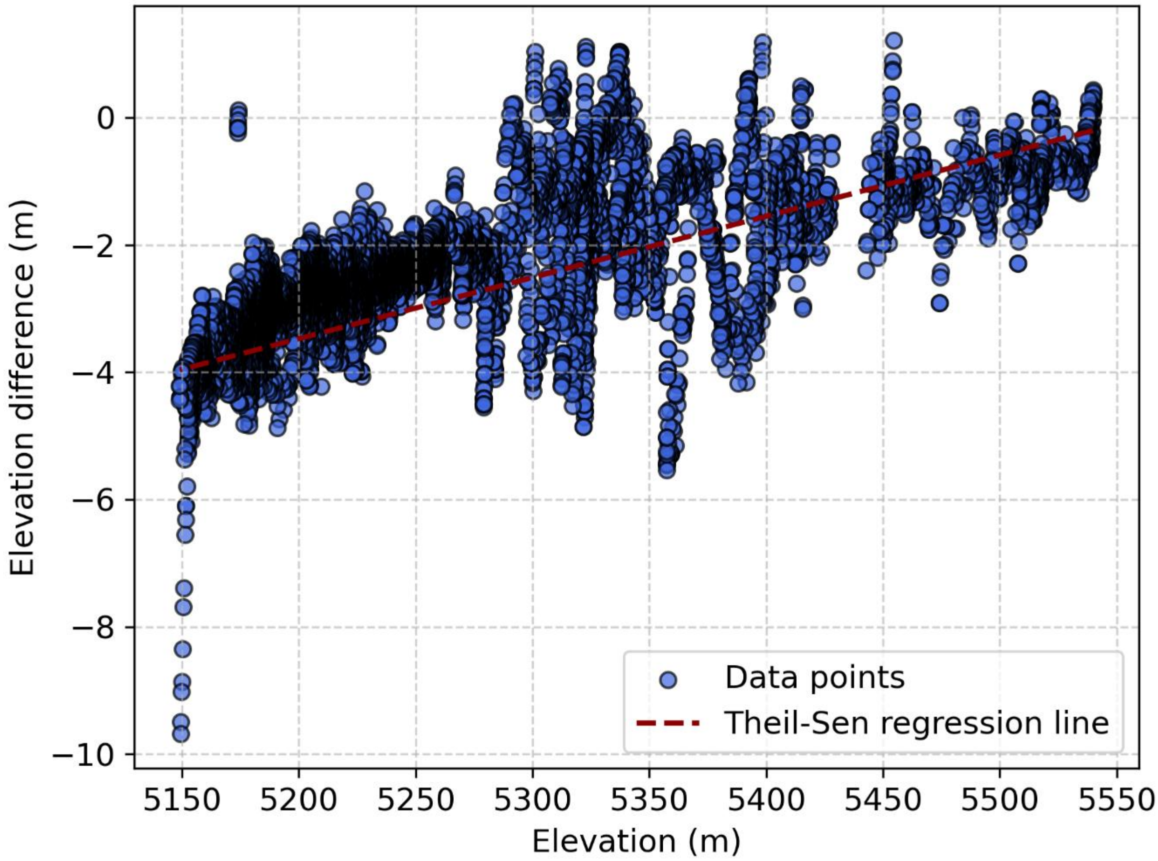

Figure 6. Glacier surface elevation changes between 2024 and 2025 generated using dGPS elevation differencing

4.2.12. Snow depth–elevation model and ΔS(z)

Snow depth change (ΔS) can be derived from stake measurements collected on two survey dates and parameterized as a function of elevation so that it can be applied consistently across the same 50 m elevation bands used for hypsometry and elevation-change integration. In such a case, stake observations consist of snow depth (m) and stake elevation (m), and the goal is to estimate representative snow depth at the midpoint of each 50 m elevation band. For Thana, the seasonal snow was present and ΔS(z) was derived from stake snow-depth data and applied in the band workflow. Snow depth is typically modelled against elevation with the robust approach used for the Δh–elevation relationship, the regression was fitted using ordinary least-squares linear regression (as implemented in the workflow) to reduce sensitivity to outliers and local variability. The fitted model for each date is then evaluated at each band midpoint to obtain $S_{t1}(z)$and $S_{t2}(z)$, and the band-wise snow depth change is computed as:

$$\Delta S(z) = S_{t2}(z) - S_{t1}(z) \quad (7)$$

4.2.13. Conversion to mass balance (point-wise and area averaged)

Geodetic mass balance was derived by converting the mean elevation-change at the mid elevation band into a specific mass-change rate. The workflow first estimates a mid-elevation change for each 50 m elevation band and even predict missing mean Δh, and (where applicable) incorporates a snow-depth term to account for differences between snow and ice density. Because seasonal snow was present during the survey period, the snow-depth term ΔS(z) was explicitly included in the band-wise geodetic mass-balance conversion to account for the density contrast between snow and ice. The resulting point-wise mass balance values are then area-weighted by the glacier's area–elevation distribution to obtain a single area averaged mean mass balance over the period $t_1$to t_2.

Annual mass balance at a point

For each 50 m elevation band z, the point-wise geodetic mass balance was computed using the formulation applied in this workflow:

$$b_{gz} = \frac{\Delta h_g(z)\,\rho_i + (S_{t2}(z) - S_{t1}(z))\,(\rho_s - \rho_i)}{(t_1)} \tag{8}$$

where $\Delta h_g(z)$is the mean elevation change for the mid elevation band, $S_{t1}(z)$and $S_{t2}(z)$are the snow depths for each mid elevation band at survey period $t_1$and t_2, and (t_1). This expression accounts for the fact that snow-depth changes contribute differently to mass change than ice-thickness changes due to the density contrast between snow and ice. The above equation yields values in kg m^{-2}; conversion to mm w.e. is described in Annex C.

Area averaged mass balance (area-weighted integration)

The area averaged mean mass balance was calculated by area-weighting the band-wise values using the glacier hypsometry:

$$\underline{b_g} = \frac{\sum_z A_z\, b_{gz}}{A_T} \tag{9}$$

where $A_z$is the glacier area within elevation band z(commonly represented as the mean band area from $t_1$and t_2, i.e., $A_z = (A_{t1} + A_{t2})/2$), and $A_T$is the total glacier area. This hypsometric integration yields a single area averaged mass-balance value representative of the full glacier surface over the observation period.

5. Uncertainty Assessment

5.1. Area averaged mass balance uncertainty

The area-average mass balance estimation is associated with three main uncertainties:

1. Uncertainty in the mass balance at each altitudinal band (db_Z; mm w.e. a^{-1}) is calculated for the bands.

2. Uncertainty from the glacier boundary delineation (dA_Z; m^2), and

3. Uncertainty from the assumed density of ice and snow (db_ρ; mm w.e. a^{-1}).

Because seasonal snow was present and ΔS(z) was included, both ice and snow density uncertainties were propagated in the uncertainty analysis. In the workflow, density uncertainties of ±30 kg m^{-3} for ice and ±100 kg m^{-3} for snow were applied, and the overall density-related uncertainty was computed from the combined ice and snow contributions (reported as Total Uncertainty Ice, Total Uncertainty Snow, and their average). The combined uncertainty (σ) is calculated following the methodology described in Tshering and Fujita (2016) as:

$$\sigma = \frac{\sum A_Z db_Z + \sum dA_Z |b_Z| + \sum A_Z db_\rho}{A_T} \quad (10)$$

Where:

- A_Z is the area within a 50 m altitudinal band,
- A_T is the total glacier area,
- b_Z is the mass balance at each band, and
- $|b_Z|$ is the absolute mass balance.

The uncertainty from the boundary delineation (dA_Z) is computed as:

dA_Z = 0.5 × pixel resolution × perimeter at each 50 m band

Given the Sentinel-2 MSI image resolution of 10 m, dA_Z is based on half the pixel size (i.e., 5 m) multiplied by the perimeter of the glacier outline at each altitudinal band (Fig.8b).

The uncertainty from the density assumption, db_{ρ}, arises from variability in the assumed densities of ice and snow. These uncertainties are averaged to represent the overall density-related uncertainty in mass balance estimation. For more details on the rationale behind the uncertainty calculation and the densities assumed, refer to Annex D.

The standard deviation (db_Z) of the mass balance across altitudinal bands, representing the uncertainty from spatial mass balance variation, is calculated as:

$$db_Z = \sqrt{\frac{1}{N}\sum(b_Z - \underline{b_z})^2} \tag{11}$$

Where N is the number of elevation bands and $\underline{b_z}$ is the mean mass balance.

6. Results and Discussion

6.1. Area averaged mass balance and uncertainty

The area averaged annual mass balance of Thana Glacier for the 2024–2025 glaciological year was estimated as -1581.676 ± 231.07 mm w.e.a^{-1}, indicating substantial net mass loss. This loss is consistent with long-term geodetic monitoring data, which indicate a sustained pattern of glacier recession since 2016. Over the nine-year observation period, Thana Glacier has consistently lost mass, showing no signs of recovery. The reported uncertainty (±231.07 mm w.e.a^{-1}) reflects the combined influence of elevation-band variability, glacier boundary delineation, and density assumptions used in the geodetic conversion (Annex A, Table A1), and provides an uncertainty-bounded estimate of recent glacier mass change under prevailing climatic conditions.

The sustained negative mass balance observed at Thana is consistent with independent evidence from Bhutan's other benchmark glaciers, indicating a coherent pattern of ongoing glacier mass loss at the national scale. For Ganglu Glacier, the 2024–2025 assessment reports an annual mass balance of −1613.876 ± 236.482 mm w.e. a^{-1}. Likewise, Shodug Glacier shows a strongly negative area averaged mass balance in 2024–2025 (geodetic estimate -2791.08 ± 390.55 mm w.e. a^{-1}), reinforcing that benchmark glaciers in Bhutan are experiencing persistent net ablation.

Table 1. Cumulative Glacier Mass Balance

Sl.No	**Year**	**AGMB**	**CGMB**
1	2016	-1036.8	-1036.8
2	2017	-1565.57	-2602.37
3	2018	-1259.14	-3861.51
4	2019	-2974.00	-6835.51
5	2020	-2441.71	-9277.22
6	2021	-2379.23	-11656.4
7	2022	-1912	-13568.4
8	2023	-1912	-15480.4
9	2024	-2422.86	-17903.3
10	2025	**-1581.68**	**-19484.98**

Beyond Bhutan, long-term benchmark observations elsewhere in the HKH similarly indicate persistent negative mass balance: Rikha Samba Glacier (central Himalaya, Nepal) has recorded negative balances in recent observational periods (e.g., -0.39 ± 0.32 m w.e. a^{-1} for 2011–2021; Gurung et al., 2023) and re-analyzed long-term series for Chhota Shigri Glacier (western Himalaya, India) reports negative geodetic mass balances for both 2003–2014 (-0.38 ± 0.05 m w.e. a^{-1}) and 2014–2020 (-0.51 ± 0.06 m w.e. a^{-1}) and a negative mean over 2002–2023 (-0.47 ± 0.19 m w.e. a^{-1}; Azam et al., 2024). Although observation periods and methods differ among studies, the consistent sign of mass balance (negative) across Bhutan and the wider HKH supports interpreting Thana's measured mass loss as part of a broader, regionally coherent response to recent climate forcing rather than a site-specific anomaly.

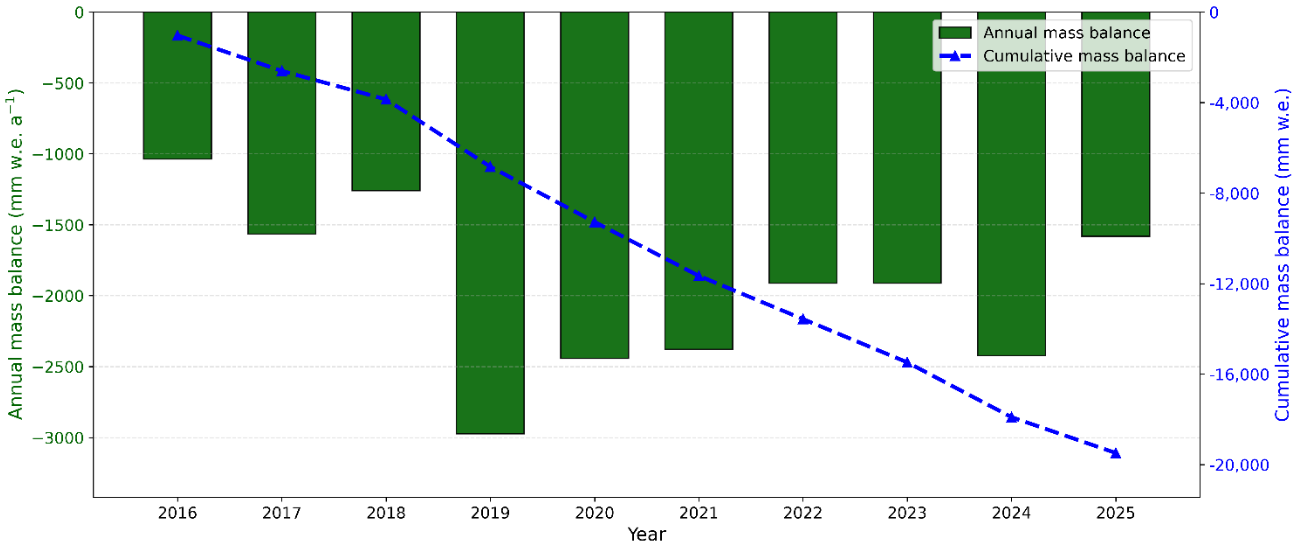

Figure 8. Cumulative mass balance and annual mass balance over the observed periods

6.2. Elevation-dependent surface lowering and hypsometric control

The frequency distribution of elevation differences (Δh) (Figure 9) is centered on negative values, with mean elevation difference of −2.54 m, indicating widespread surface lowering across Thana Glacier. Elevation-band analysis (Annex A, Table A1) refines this area averaged signal and shows a clear elevation dependence, with stronger thinning at lower elevations and reduced thinning toward higher elevations: the lowest elevation band (5,133–5,183m a.s.l.) recorded a mean Δh of −3.44 m, whereas the highest band (5,533–5,583 m a.s.l.) showed a smaller mean Δh of −0.834 m. When integrated hypsometrically, the mid-elevation band (5,183–5,233 m a.s.l.) contributed the largest share (-567.94 mm w.e. a^{-1}) to the area averaged mass balance because it contains the largest fraction of the glacier area (≈24%), demonstrating that the overall mass-balance signal is strongly influenced by the glacier's hypsometry rather than by thinning magnitude alone.

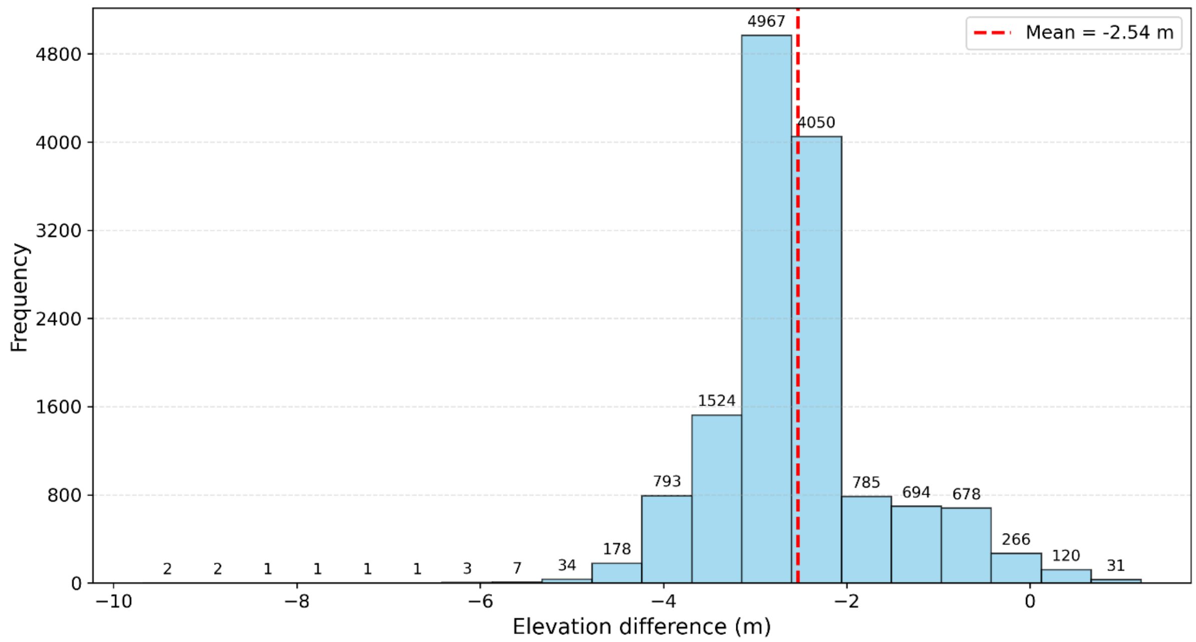

Figure 9. Distribution of glacier surface elevation change between 2024 and 2025.

6.3. Glacier area change

Using the 2025 Sentinel-2 median composite (10 m) and manual digitization in QGIS, the mapped planimetric extent of Thana Glacier for the year 2024-2025 assessment is 3.473 km² (3,472,921 m²; 347.29 ha). This glacier outline polygon was used to clip the vertically corrected DEM and to derive the glacier hypsometry (area distribution by 50 m elevation bands) for subsequent area-weighted integration.

The hypsometric analysis indicates that the glacier area is concentrated in the mid-elevation zone: the 5,183-5,233 m a.s.l. band contains the largest fraction of the glacier area (about 24%), while progressively smaller areas occur toward the highest elevation bands. This topographic distribution is important because it modulates the glacier-wide mass balance: elevation bands with both large area and strong thinning exert the greatest influence on the area-averaged signal.

In the previous assessment (2023-2024), the glacier area was reported as approximately 3.70 km² and the study noted a total reduction of 3.87% in glacier surface area since 2016. The continued negative mass balance and observed terminus retreat during 2024-2025 indicate that long-term areal shrinkage is expected to persist. For a robust estimate of annual planimetric area change between 2024 and 2025, year-specific outlines should be delineated consistently from comparable imagery and field-checked terminus mapping, and their areas compared.

6.4. Mass-balance gradient and ELA interpretation (2024–2025)

The mass-balance profile for Thana Glacier (2024–2025), derived from elevation-band observations (50 m bands; midpoints ~5158–5658 m a.s.l.), demonstrates a strong and systematic elevation control on net balance across the surveyed elevation range. Band balances are markedly negative at low elevations and progressively become less negative with increasing elevation, indicating a consistent reduction in net ablation or increasing accumulation with altitude. The derived band balances (seasonal_MB, mm w.e.) rise from approximately −2959 mm w.e. at ~5158 m to −280 mm w.e. at ~5558 m, approaching near-zero conditions toward the glacier's highest elevations. This behavior is consistent with a robust altitudinal gradient in surface mass balance, where the lower glacier experiences strong mass loss while the upper glacier approaches balance.

A linear regression of elevation-band mass balance as a function of elevation, expressed as $b_{gz}(z) = az + c$, captures this relationship well over the analysed range and provides a compact description of the glacier's elevation sensitivity. The fitted slope represents the mass-balance gradient, db/dz, and for Thana Glacier (2024–2025) the notebook-derived band profile implies a gradient of approximately $+6.0$mm w.e. m^{-1} (equivalent to ~0.60 m w.e. per 100 m). This indicates that an increase of 100 m in elevation improves the net balance by roughly 0.6 m w.e., reflecting strong elevation moderation of ablation and increasing snowfall retention with height. The near-linear character of the profile suggests that, within the analysed elevation range, the combined effects of melt energy, debris/albedo conditions, and snow accumulation can be reasonably approximated by a first-order elevation dependence.

The equilibrium line altitude (ELA) is estimated from the zero-crossing of the fitted profile ($b_{gz} = 0$). Based on the band-balance profile, the transition from negative to near-zero/positive balance occurs near the upper glacier, yielding an ELA of approximately ~5605 m a.s.l. Notably, the ELA estimate is constrained by the highest observed negative band (~5558 m), but the first slightly positive band occurs in an elevation band where paired point observations were absent and values are extrapolated in the notebook; therefore, the ELA should be interpreted as a fitted/model-based balance ELA for the 2024–2025 period rather than a directly bracketed observational crossing. Despite the ELA lying within the glacier's elevation envelope, it is positioned very near the top of the glacier hypsometry, implying that only a small fraction of glacier area lies above the equilibrium line and that the glacier remains predominantly ablation-dominated overall. Consistent with this, the area-weighted integration of band balances yields a glacier-wide mass balance of −1581.68 mm w.e. for 2024–2025 (with the notebook-reported overall uncertainty of ~±231 mm w.e.), confirming substantial net mass loss even under a strong elevation-dependent balance structure.

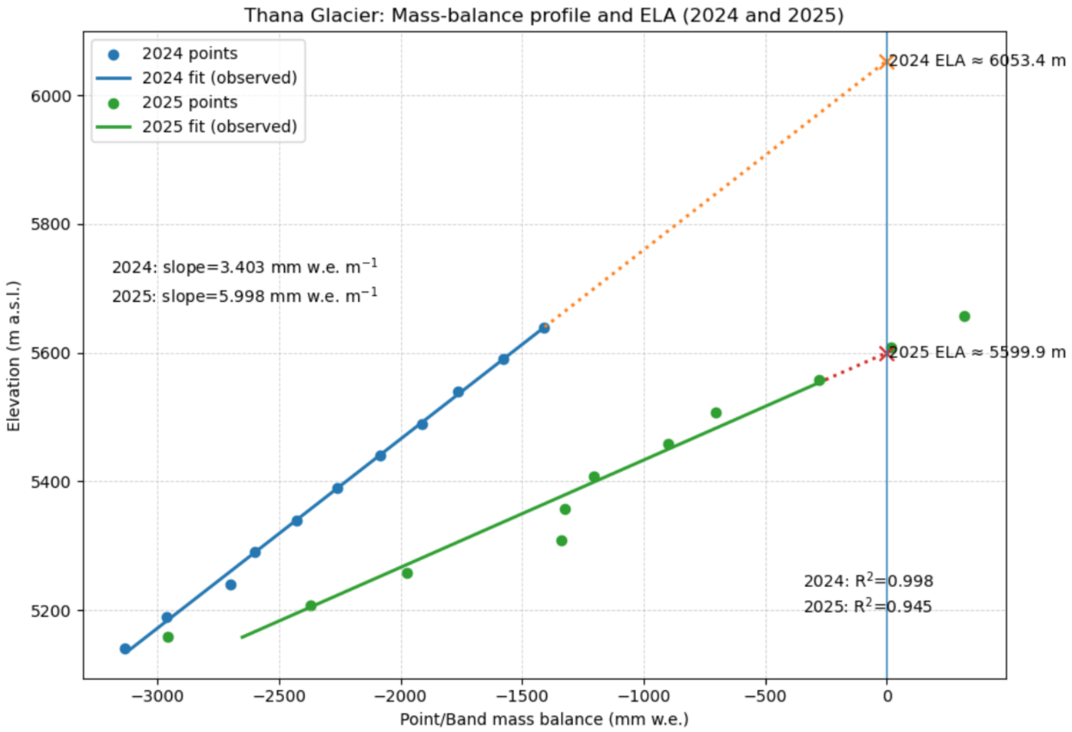

Figure 10. Equilibrium-line altitude (ELA) for 2024 and 2025.Observed point mass balance (mm w.e.) versus elevation (m a.s.l.), with solid line as linear fit and dotted line showing extrapolation

6.5. Cumulative terminus recession

Mapping of the Thana Glacier terminus over 2023–2025 indicates a clear and coherent pattern of frontal retreat, quantified from multiple transects drawn orthogonal to the ice front. The one-year recession between 2024 and 2025 ranges from 10.1 to 51.74 m (mean ~23.9 m), whereas the cumulative displacement between 2023 and 2025 increases to 17.4–103.53 m (mean ~49.4 m, ~24.7 m a^{-1} when annualized), demonstrating sustained retreat over consecutive years rather than an isolated positional shift. The magnitude and persistence of this retreat provide strong geometric evidence of ongoing glacier adjustment to a negative mass-balance regime, that is ablation at the tongue exceeds replenishment by ice flux from the upper part of the glacier. The maximum retreat exceeding 100 m at one transect, further suggests that the response is locally modulated by terminus geometry and surface conditions, such as debris thickness contrasts, meltwater routing, and uneven down wasting, superimposed on an overall climate-driven tendency toward enhanced melt and reduced frontal stability.

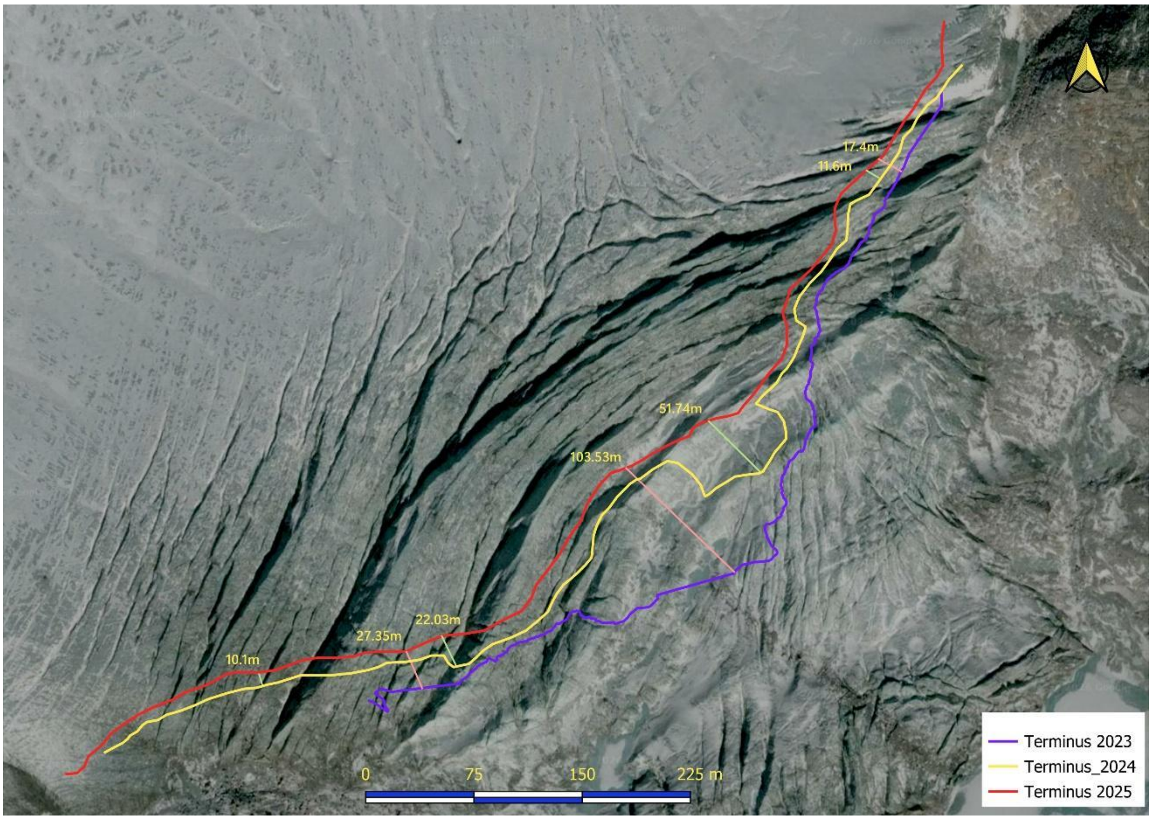

Figure 11. Cumulative terminus positions of Thana Glacier from 2023 to 2025. The progressive upstream displacement of the terminus outline

7. References

Azam, M. F., Vincent, C., Srivastava, S., Berthier, E., Wagnon, P., Kaushik, H., Hussain, M. A., Munda, M. K., Mandal, A., & Ramanathan, A. (2024). Reanalysis of the longest mass balance series in Himalaya using a nonlinear model: Chhota Shigri Glacier (India). *The Cryosphere, 18*, 5653–5672. https://doi.org/10.5194/tc-18-5653-2024

Barry, R. G. (2006). *The status of research on glaciers and global glacier recession: A review*. *Progress in Physical Geography: Earth and Environment*, 30(3), 285–306. https://doi.org/10.1191/0309133306pp478ra

Gurung, T. R., Kayastha, R. B., Fujita, K., Joshi, S. P., Sinisalo, A., & Kirkham, J. D. (2023). A long-term mass-balance reconstruction (1974–2021) and a decadal in situ mass-balance record (2011–2021) of Rikha Samba Glacier, central Himalaya. *Journal of Glaciology, 69*(276), 723–736. https://doi.org/10.1017/jog.2022.93

Hugonnet, R., McNabb, R., Berthier, E., Menounos, B., Nuth, C., Girod, L., Farinotti, D., Huss, M., Dussaillant, I., Brun, F., & Kääb, A. (2021). Accelerated global glacier mass loss in the early twenty-first century. *Nature, 592*(7856), 726–731. https://doi.org/10.1038/s41586-021-03436-z

Immerzeel, W. W., Van Beek, L. P. H., & Bierkens, M. F. P. (2010). Climate change will affect the Asian water towers. *Science*, 328(5984), 1382–1385. https://doi.org/10.1126/science.1183188

Intergovernmental Panel on Climate Change (IPCC). (2023). *Climate change 2023: Synthesis report. Contribution of Working Groups I, II and III to the Sixth Assessment Report of the Intergovernmental Panel on Climate Change*. https://www.ipcc.ch/report/sixth-assessment-report-cycle/

Kraaijenbrink, P. D. A., Bierkens, M. F. P., Lutz, A. F., & Immerzeel, W. W. (2017). Impact of a global temperature rise of 1.5 °C on Asia's glaciers. *Nature*, 549(7671), 257–260. https://doi.org/10.1038/nature23878

National Center for Hydrology and Meteorology. (2018). *Bhutan glacier inventory 2018*. Royal Government of Bhutan. ISBN: 978-99980-862-2-7

National Center for Hydrology and Meteorology. (2024). *Annual report 2023–2024*. Royal Government of Bhutan.

National Snow and Ice Data Center (Comp.). (2002, updated 2021). *Glacier photograph collection, version 1* [Data set]. NSIDC. https://doi.org/10.7265/N5/NSIDC-GPC-2009-12

The GlaMBIE Team. (2025). Community estimate of global glacier mass changes from 2000 to 2023. *Nature, 639*, 382–388. https://doi.org/10.1038/s41586-024-08545-z

Tshering, P., & Fujita, K. (2015). First in situ record of decadal glacier mass balance (2003–2014) from the Bhutan Himalaya. *Annals of Glaciology*, 57(71), 289–294. https://doi.org/10.3189/2016aog71a036

World Glacier Monitoring Service. (2025). *Fluctuations of Glaciers (FoG) database* (Version 2025-02b) [Data set]. WGMS. https://doi.org/10.5904/wgms-fog-2025-02b

World Meteorological Organization. (2023). *State of the global climate 2023*. https://public.wmo.int/en/our-mandate/climate/wmo-statement-state-of-global-climate

World Meteorological Organization. (2025). *State of the global climate 2024* (WMO-No. 1368). WMO. https://library.wmo.int/idurl/4/69495

8. Annexture

8.1. Annex A: Hypsometric elevation-band statistics and point mass balance

Table A1 summarizes elevation-band (hypsometric) elevation differences (Δh), derived areas, perimeter, and point mass balance outputs used in the geodetic mass balance workflow.

Elevation band (m a.s.l.)	**Mid-elevation (m)**	**Pixel count**	**Mean Δh (m)**	**Mean band area (m²)**	**Area (%)**	**Perimeter (m)**	**Point mass balance (mm w.e.)**	**Area-weighted MB contribution (mm w.e.)**	**Uncertainty (Ice)**	**Uncertainty (Snow)**
5133–5183	5158	2384	-3.439	161,315.65	4.64	1,875.59	-2,959.02	-137.445	10.78	14.558
5183–5233	5208	6152	-2.799	832,656.02	23.98	1,815.39	-2,368.83	-567.944	47.717	64.501
5233–5283	5258	2847	-2.344	606,673.02	17.47	1,091.94	-1,975.68	-345.126	33.512	45.481
5283–5333	5308	950	-1.612	270,997.84	7.8	836.3	-1,339.54	-104.527	14.869	20.221
5333–5383	5358	592	-1.584	352,252.97	10.14	750.92	-1,323.13	-134.203	20.488	27.873
5383–5433	5408	440	-1.442	401,273.85	11.55	1,072.62	-1,205.81	-139.323	21.968	29.865
5433–5483	5458	265	-1.085	266,203.37	7.67	1,800.57	-899.52	-68.949	14.967	20.336
5483–5533	5508	401	-0.855	355,706.43	10.24	1,540.38	-704.464	-72.153	19.834	26.976
5533–5583	5558	107	-0.364	158,963.88	4.58	1,512.17	-280.311	-12.83	8.44	11.493
5583–5633	5608	0	-0.016	61,387.77	1.77	678.1	18.346	0.324	3.223	4.394
5633–5683	5658	0	0.332	5,490.46	0.16	111.23	316.509	0.5	0.272	0.371
TOTAL / glacier-wide	—	—	—	**3,472,921.24**	**100**	—	—	**-1,581.68**	—	—

Summary Statistics:

- Total Area Average: 3,472,921.242 m² (≈ 3.4729 km²)

- Total Uncertainty Ice: 196.07 mm w.e.

- Total Uncertainty Snow: 266.07 mm w.e.

- Overall Uncertainty Average: 231.07 mm w.e.

- Area wide mass balance (area-weighted SMB/AGMB): −1581.676 mm w.e. (≈ −1.582 m w.e.)

8.2. Annex B: Physical Assumptions

Densities used

The following densities were applied for the geodetic mass balance measurement:

- **Ice density:** $\rho_i \approx 880\ kg\ m^{-3}$
- **Snow density:** $\rho_s \approx 400\ kg\ m^{-3}$
- **Water density:** $\rho_w \approx 1000\ kg\ m^{-3}$

8.3. Annex C: Unit equivalence used in mass-balance calculations

In glacier mass-balance studies, mass changes are commonly expressed either as mass per unit area (kg m⁻²) or as millimeters of water equivalent (mm w.e.). These two units are directly and numerically equivalent due to the physical relationship between mass, area, thickness, and the density of liquid water.

Mass balance expressed in kg m⁻² represents the amount of mass gained or lost per square meter of glacier surface. When this mass is converted to an equivalent thickness of water, the relationship is given by:

$$h = \frac{m}{\rho_w}$$

where

h= equivalent water thickness (m),

m= mass per unit area (kg m⁻²), and

ρ_w= density of liquid water (≈ 1000 kg m⁻³).

For a mass change of 1 kg m⁻²:

$$h = \frac{1\ kg\ m^{-2}}{1000\ kg\ m^{-3}} = 0.001\ m = 1\ mm$$

Thus, a mass of 1 kg uniformly distributed over an area of 1 m^2 corresponds to a water layer of 1 mm thickness. This leads to the direct numerical equivalence:

$$1\ kg\ m^{-2} = 1\ mm\ w.e.$$

As a result, glacier mass-balance values reported in kg m^{-2} can be directly expressed in millimeters of water equivalent without further scaling, provided the reference density is that of liquid water. This convention allows glacier mass changes to be interpreted intuitively as an equivalent water depth and facilitates comparison across glaciers of different sizes.

8.4. Annex D: Snow and ice density uncertainty in mass-balance calculations.

In the conversion of elevation change to mass balance, assumed densities for glacier ice and snow introduce an additional source of uncertainty. These densities are not constant; they vary spatially and temporally due to differences in internal structure, compaction, temperature, and metamorphic processes. To account for this variability, density-related uncertainties were explicitly included in the uncertainty propagation. Reference densities for glacier ice and snow were adopted as specified in Annex C. For the current study, seasonal snow was present during the survey period and was explicitly incorporated through the ΔS(z) term; therefore, uncertainty contributions from both ice and snow densities were included in the final uncertainty calculation. Density uncertainties of ±30 kg m^{-3} (ice) and ±100 kg m^{-3} (snow) were applied following common ranges reported in glaciological studies and consistent with the workflow implementation.

NATIONAL CENTRE FOR HYDROLOGY AND METEOROLOGY

ROYAL GOVERNMENT OF BHUTAN

www.nchm.gov.bt